Modeling Asphaltene Deposition in Production Pipelines

E. Ramirez-Jaramillo,[†] C. Lira-Galeana,*[,†] and O. Manero[‡]

Mexican Institute of Petroleum, Mexico City, 07730, Mexico, and National University of Mexico, Mexico City, 04250, Mexico

Received August 16, 2005. Revised Manuscript Received December 27, 2005

A multiphase (oil/gas/asphaltene/water) multicomponent hydrodynamic model is proposed to represent the phenomenon of asphaltene deposition in producing wells. The model is based on the assumption that asphaltene particles are thermodynamically formed at a given set of $p-T-x$ conditions during the flow, and both molecular diffusion and shear removal are two competing mechanisms that define the radial diffusion and later deposition of asphaltene particles for either turbulent or laminar flows in a well. Predictions of the model are presented for the case of two problematic (plugged) wells from the southwest producing area of Mexico, where measured pressure−temperature−depth production profiles related to deposits are available.

Introduction

Asphaltene deposition in producing wells, pipes, and surface facilities has been an outstanding problem with wide economic impact to the oil industry. To reduce the number of operations intended to clean the producing wells from depositions, a great deal of resources are directed nowadays to predict and prevent both the time and extent in which such depositions may affect a producing asset.

Solid deposits caused by asphaltenes have led to a great number of technical and operative problems. Due to the high-pressure levels at the bottom of some wells and the steep angle of inclination of some directional systems, the use of real-time tools to monitor depositions downhole presents a great difficulty. In some of the cases, interference of the detection device with the flow of hydrocarbons may induce the deposition, as it alters the pressure drop, then destabilizes the system, causing solid blockage and even the loss of the tool and, in critical cases, of the entire well. Among various issues, the lack of information regarding the deposition depth in producing wells is a major problem.[1,2]

Surface facilities such as pumps, tubes, valves, fittings, tanks, and so forth can also be affected by asphaltene depositions in cases where the deposition conditions are located near the well surface.

In this regard, a predictive model for asphaltene deposition applied to real production conditions is thus of significant importance.

Modeling of the heavy organic deposition in flowing conditions has received special attention, especially that of wax deposition in flowlines.[3−10] In contrast, the literature on models for multiphase transport of asphaltenic crudes is practically void, and only one model can be found in the literature.[11,39]

Most of the two-phase (gas−liquid) flow simulations in pipes are based on experimental correlations for heavy hydrocarbons (black oils) which allow determination of the phase behavior and pressure profiles with confidence. On the other hand, for light oils the same correlations cannot be used. Nowadays, multiphase-flow semiempirical correlations with the conservation equations are used to calculate pressure and temperature profiles for design of production pipes.[13,14]

Mathematical models that describe the flow of hydrocarbons in pipes can be classified into two categories: The so-called *mechanistic* models (which use experimental correlations) based on the "black oil" formulation[13] and those named compositional models, which use equations of state to predict phase equilibrium.[15,16] In the former, black oil stands for a homogeneous liquid hydrocarbon mixture, which is in equilibrium with a gas phase under decreasing temperature and pressure. The two phases are considered as one-component systems with properties depending on pressure and temperature, calculated from experimental correlations. This model may be applied to heavy oils with API density less than 20. It may also be applied to light saturated oils if a correlation to determine the saturation pressure is available.[17]

* Corresponding author. Phone: (+52)-55-9175-6507. Fax: (+52)-55-9175-7225. E-mail: clira@imp.mx.

[†] Mexican Institute of Petroleum.

[‡] National University of Mexico.

(1) Kokal, S. L.; Sayegh, S. G. Asphaltenes: The Cholesterol of Petroleum. Presented at the SPE Middle East Oil Show, Bahrain, March 11−14, 1995; Society of Petroleum Engineers: Houston, TX, 1995; SPE No. 29787, pp 169−181.

(2) Creek, J. L. *Energy Fuels* **2005**, *19*, 1212−1224.

(3) Brown, T. S.; Nielsen, V. G.; Erickson, D. D. *SPE Prod. Eng.* **1993**, 353−368; SPE No. 26548.

(4) Burger, E. D.; Perkins, T. K.; Striegler, J. H. *JPT* **1981**, 1075−1086.

(5) Hsu, J. J. C.; Santamaria, M. M. *SPE Prod. Eng.* **1994**, 179−192; SPE No. 28480.

(6) Hunt, J. *J. Pet. Technol.* **1962**, *225*, 1259−1267.

(7) Majeed, A.; Bringedal, B.; Overa, S. *Oil Gas J.* **1990**, *18*, 63−69.

(8) Singh, P.; Venkatesan, R.; Fogler, H. S.; Nagarajan, N. *AIChE J.* **2000**, *46*, 1059−1074.

(9) Weingarten, J. S.; Euchner, J. A. *SPE Prod. Eng.* **1988**, 121−126.

(10) Ramirez-Jaramillo, E.; Lira-Galeana, C.; Manero, O. *Pet. Sci. Technol.* **2004**, *22*, 821−861.

(11) Leontaritis, K. J. *SPE Prod. Eng.* **1997**, 277−288; SPE No. 39446.

(12) Lira-Galeana, C.; Ramírez-Jaramillo, E.; Buenrostro-González, E.; Manero, O.; Ortega-Rodríguez, A.; Alvarez-Robles, L. Internal Report; F. 53937; Instituto Mexicano del Petróleo: Mexico, 2003.

(13) Bendiksen, K. H.; Maines, D.; Moe, R.; Sven, N. *SPE Prod. Eng.* **1991**, 171−180; SPE No. 19451.

(14) Ansari, A. M.; Sylvester, N. D.; Sarica, C.; Shoham, O.; Brill, J. P. *SPE Prod. Eng.* **1994**, *297*, 363−367; SPE No. 20630.

(15) Gould, T. L. *SPE Prod. Eng.* **1985**, 373−384; SPE No. 5685.

(16) Adewumi, M. A.; Mucharam, L. *SPE Prod. Eng.* **1990**, 85−90.

(17) Brill, J. P.; Airachakaran, S. J. *JPT* **1992**, 538−541.

10.1021/ef050262s CCC: $33.50
Published on Web 03/10/2006

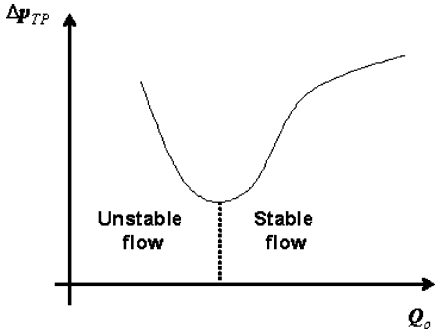

Figure 1. Pressure drop behavior as a function of oil flow rate in vertical flow.

Table 1. Pressure Drop Contributions during the Flow of Produced Hydrocarbons in an Oil Well

productivity index*10^{-9} J [$(m^3/s)/(kg/m^2)$]	Q_o (m^3/s)	Q_o (BPD)	% pressure drop		
			reservoir	well	surface
6.54	0.005	2700	36	59	5
13.1	0.007	3700	25	69	6
26.2	0.008	4500	15	78	7
26.2	0.009	4800	11	81	8

Determination of pressure drop in vertical pipes is important, since by these drops the available energy of the well is consumed. In Table 1, the contribution to the total energy consumption of the pressure drop is explicitly presented.

In Figure 1, the total pressure drop is plotted with the vertical liquid flow rate. In the stable flow region, pressure drops increase with flow rate due to friction losses, while in the unstable flow region pressure drops increase with the reduction in flow rate. This is due to the holdup increase and hence to the increase in pressure drop caused by an increase in density.

Model for Asphaltene Deposition in a Well

A transport model for asphaltene deposition that incorporates a four-phase (asphaltene−oil−vapor−water) interacting system, a rheological equation of state, and semiempirical correlations for multiphase flow is described in the following sections. Predictions of the model include the deposited mass profiles as a function of time and position. The effect of the flow regime on deposition is analyzed in detail, including the change in the rheological properties as the liquid flows along the pipe. One form of this model has been previously presented for a waxy-type liquid−solid flow,[10] and its generalization for the three-phase flow involving asphaltene deposition is presented here. The model considers molecular diffusion of asphaltene aggregates in the radial direction, neglecting any electrokinetic phenomena.[18]

Figure 2 presents the flow system schematically. A pipe region of dimensions r and z and length L contains a flowing liquid with initial composition. The fluid is a hydrocarbon mixture of n-components, and thus the mol fractions of the different phases (liquid, solid, gas, and water, if present) are functions of pressure and temperature at a given pipe location (see the Nomenclature section for a description of variables).

The pipe has an inner radius r_o and transports a multicomponent hydrocarbon mixture that enters the bottom of the pipe at an initial pressure p_o, temperature T_o, and volumetric flow rate Q_o. The exterior temperature of the pipe and the fluid pressure change along the length of the pipe, and consequently

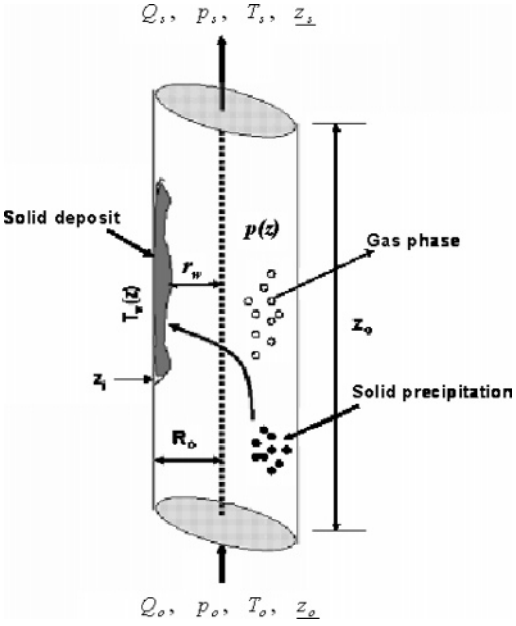

Figure 2. Solid deposition in a model pipe.

the fluid is cooled and expanded as it follows its upward motion. The forced-convection heat-transfer process induces a change in the liquid temperature; $r_w(t,z)$ is the effective pipe radius that includes the deposited solids layer. The dissolved asphaltene diffuses radially by molecular diffusion. It is precipitated on the wall surface, and as soon as the layer is formed, it is subjected to external forces (shear-removal forces) due to shear flow.

In the case where the oil flow is in the turbulent regime, an assumption on the presence of a laminar sublayer is made. The flow regions in this case include a turbulent core, a transition zone, and the laminar sublayer. In the turbulent core, heat transport is fast and the radial variation of the temperature profile is negligible. In the region next to the wall, heat conduction across the laminar sublayer is assumed, and hence a more pronounced temperature drop occurs. In the transition zone, heat conduction and turbulent heat transport are present. Figure 3 shows a typical temperature profile under these conditions.[19]

The wall temperature, and hence that of the laminar sublayer, is always lower than the core temperature. This further supports the assumption of molecular diffusion induced by the presence of a radial temperature gradient. The wall temperature may be calculated according to:

$$T_{wall} = T_{fluid} - \frac{Q}{h_{in}A} \tag{1}$$

where T_{fluid} is the mean temperature in the core, Q is the heat flux, A is the inner surface, and h_{in} is the heat transfer coefficient that changes according to the type of flow:[20]

$$h_{in} = 0.026\frac{k_b}{D}\left(\frac{D\rho_m v_s}{\eta_b}\right)^{0.8}\left(\frac{C_p\eta}{k_b}\right)^{1/3}\left(\frac{\eta_b}{\eta_o}\right)^{0.14} \quad Re > 20\,000 \tag{2}$$

$$h_{in} = 1.86\frac{k_b}{D}\left(Re\,Pr\frac{D}{L}\right)^{1/3}\left(\frac{\eta_b}{\eta_o}\right)^{0.14} \quad Re < 20\,000 \tag{3}$$

where D and L are the pipe diameter and length, respectively,

(18) Gonzalez, G.; Guilherme, B. M. N.; Sandra, M. S.; Elizabete, F. L.; dos Anjos de Sousa, M. *Energy Fuels* **2003**, *17*, 879−886.

(19) Bird, R. B.; Stewart, W. E.; Lightfoot, E. N. *Transport Phenomena*; Wiley: New York, 1987; Ed. Reverté.

(20) Sieder, E. N.; Tate, G. E. *Ind. Eng. Chem.* **1936**, *28*, 1429−1435.

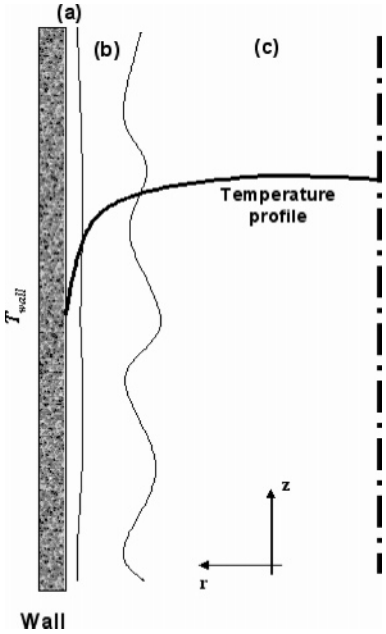

Figure 3. Temperature change in: (a) laminar layer, (b) transition zone, and (c) turbulent core.

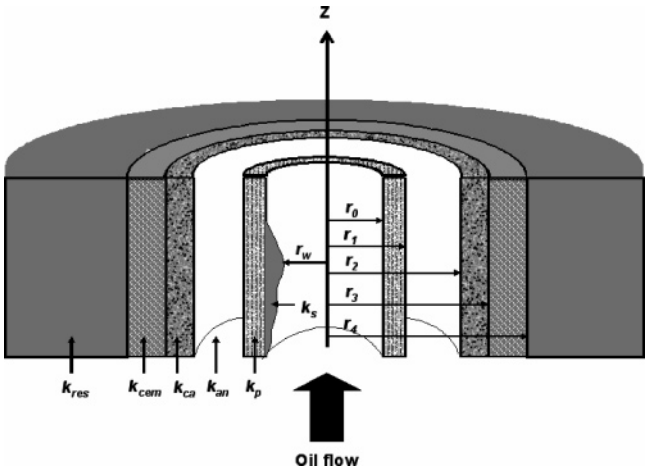

Figure 4. Heat transfer model in a well.

Re and *Pr* are the Reynolds and Prandtl numbers, respectively, C_p is the heat capacity of the mixture, and η_b and k_b are the viscosity and thermal conductivity of the mixture, respectively. In eq 1, the total heat flux (Q) is a function of the global heat transfer coefficient (U), which can be expressed according to:

$$U = \frac{1}{r_w}\left(\frac{1}{k_{cem}}\ln\frac{r_4}{r_3} + \frac{1}{k_{ca}}\ln\frac{r_3}{r_2} + \frac{1}{k_{an}}\ln\frac{r_2}{r_1} + \frac{1}{k_p}\ln\frac{r_1}{r_0} + \frac{1}{k_s}\ln\frac{r_0}{r_w} + \frac{1}{h_{in}r_w}\right)^{-1} \quad (4)$$

r_i and k_j are illustrated in Figure 4. k_s is the thermal conductivity of the solid deposit given by:[8]

$$k_s = \frac{\lfloor 2k_\beta + k_{oil} + (k_\beta - k_{oil})F_w \rfloor}{[2k_\beta + k_{oil} - 2(k_\beta - k_{oil})F_w]}k_{oil} \quad (5)$$

where β is the caloric resistance of asphaltenes, k_{oil} is that of the oil, and F_w is the solids weight fraction.

Thermodynamic Model for Asphaltene Precipitation. The thermodynamic model for asphaltene precipitation used in this work is the one described by Buenrostro-González et al.,[21] in which the oil is assumed as a structureless continuum and its properties such as dielectric constant, density, or Hamaker constant vary continuously in that domain. The phase equilibrium (oil−gas−asphaltene separation) is described by a modified version of the statistical association fluid theory for potentials of variable range (SAFT-VR) EOS.[22] The solution to the phase equilibrium/mass balance equations gives the conditions and amount of asphaltene precipitated from the reservoir fluid at a given set of pressure, temperature, and composition for a given flow cell in which the production tubing is divided for analysis.

In the SAFT-VR EOS described by Buenrostro-González et al.,[21] the total Helmholtz free energy for associating chain molecules is given by:[22−24]

$$\frac{A_H}{N_m kT} = \frac{A_H^{Ideal}}{N_m kT} + \frac{A_H^{Mono}}{N_m kT} + \frac{A_H^{Chain}}{N_m kT} + \frac{A_H^{Assoc}}{N_m kT} \quad (6)$$

where A_H includes all the different contributions to the free Helmholtz energy (ideal, monomers, chain, and association), N_m is the number of molecules, k is the Boltzmann constant, and T is the temperature.

Transport Model

The constitutive equation for the fluid is the modified Casson equation of state:

$$\tau = 2\eta(\Pi_D, w_s)D \quad (7)$$

where τ and D are the stress and the rate of deformation tensors, respectively, and $\eta(\Pi_D, w_s)$ is the viscosity as a function of the second invariant of the rate of deformation tensor (Π_D) and the weight fraction of the solid phase. The use of the Casson equation of state for asphaltene solutions is one of the possible choices among various rheological models. Oil solutions with precipitated solids present yield stresses especially when they have high molecular weight tails, and they present time-dependent phenomena as the structure gradually brakes down at high shear rates. Initially, the flow curve can be represented by a Bingham plastic model, but as shearing proceeds, a limiting curve is reached and can be represented by the nonlinear Hershel−Bukley or Casson models. The latter model was chosen because a wealth of data from complex oils is provided.

The dependence of the viscosity with shear rate and concentration for multicomponent hydrocarbon mixtures has been suggested by Pedersen and Ronningsen:[25]

$$\eta = \eta_{liq}\exp(\lambda_1\Phi_{solid}) + \frac{\lambda_2\Phi_{solid}}{\sqrt{\dot\gamma}} + \frac{\lambda_3\Phi_{solid}^4}{\dot\gamma} \quad (8)$$

where $\dot\gamma$ is the shear rate and Φ_{solid} is the solid fraction; η_{liq} corresponds to the dilute limit of the suspension viscosity ($\Phi_{solid} \rightarrow 0$). Parameters λ_1, λ_2, and λ_3 are constants to be determined for each oil. In this work, we took the following values:[25] $\lambda_1 = 37.82$, $\lambda_2 = 83.96$, and $\lambda_3 = 8.559 \times 10^6$.

(21) Buenrostro-Gonzalez, E.; Lira-Galeana, C.; Gil-Villegas, A.; Wu, J. *AIChE J.* **2004**, *50*, 2552−2570.
(22) Chapman, W. G.; Gubbins, K. E.; Jackson, G.; Radosz, M. *Fluid Phase Equilib.* **1989**, *52*, 31−38.
(23) Chapman, W. G.; Gubbins, K. E.; Jackson, G.; Radosz, M. *Ind. Eng. Chem. Res.* **1990**, *29*, 1709−1721.
(24) Wu, J.; Prausnitz, J. M.; Firoozabadi, A. *AIChE J.* **1998**, *44*, 1188−1199.
(25) Pedersen, K. S.; Ronningsen, H. P. *Energy Fuels* **2000**, *14*, 43−51.

Table 2. Classification of Correlations Used

category	correlations	application range	flow regime
I	Poettmann and Carpenter[37] Baxendell and Thomas[38] Fancher and Brown[39]	black oil light oil	No distinction for different flow regimes.
II	Hagedorn and Brown[40] (With either the original calculation of the saturation pressure or with the Griffith & Wallis correction for H_{LNS})	light oil	No distinction for different flow regimes.
III	Duns and Ros[41] Orkiszewski[42] Beggs and Brill[43] (Using the Palmer's correction for H_L or without correction) Dukler et al.[44] (Using the Eaton or Dukler method to calculate H_L) Murkherjee and Brill[45] Aziz, Govier, and Fogarasi[46] Cullender and Smith[47]	black oil light oil gas and condensate	*Bubble flow* *Slug flow* *Transition flow* *Mist flow*

The fluid pressure drop in a vertical pipe is the sum effect of the energy lost friction, the change in potential energy, and the change in kinetic energy. This energy balance, which is basic to all pressure-drop calculations, can be generally written as:

$$\left(\frac{\Delta p}{\Delta L}\right)_T = \left(\frac{\Delta p}{\Delta L}\right)_{ac} + \left(\frac{\Delta p}{\Delta L}\right)_e + \left(\frac{\Delta p}{\Delta L}\right)_f \quad (9)$$

which means that the total pressure gradient includes the contributions of the acceleration (ac), elevation (e), and friction (f).

A characteristic property of multiphase flow is the presence of flow regimes representing the distribution of phases inside the pipe. Various flow patterns are found depending on pressure and temperature conditions, flow rate, pipe diameter, and fluid properties. This complexity is due to changes in composition, flow rate, physical properties of each phase resulting from the pressure drop, and heat transfer with the surroundings. Most investigators who consider flow regimes define four regimes (bubble flow, slug flow, transition flow, and mist flow) which may occur in a vertical pipe.[17] These flow regimes affect the pressure gradient which itself affects the temperature, heat transfer, and deposition process. Therefore, the flow regime is considered to affect the deposition process in an indirect manner. Nevertheless, in every flow regime, it is always possible to find a narrow laminar layer (the viscous or heat sublayer) of fluid next to the wall. Within this layer, laminar flow allows molecular diffusion of asphaltene aggregates in the radial direction. In the core, on the other hand, the temperature profile is assumed flat, and therefore the flow regime affects the deposition process through the pressure gradient, which itself is a function of the flow regime.

The redissolution kinetics of deposits due to changes in the thermal gradients with time is also an important factor in the analysis of deposition. In fact, the kinetics of aggregation or de-aggregation of asphaltenes has not been considered in the present model to a fair extent. The approach taken here is a phenomenological one in which the dissolved solids change phase and the liquid phase is depleted of solids next to the wall. Once again, the thermodynamic equilibrium is assumed to be attained at times shorter than any flow-related time scale. In this case, the phase change occurs faster than any aggregation kinetics process, and by extension, the thermodynamic conditions would control any redissolution of solids into the liquid phase.

Many correlations have been developed for predicting two-phase (gas−liquid) flowing pressure gradients that differ in the manner used to calculate these three components of the total pressure gradient (eq 9). Some investigators chose to assume that the gas and liquid phases travel at the same velocity (no slip between phases) for evaluating the mixture density and evaluate only a friction factor empirically. Others developed methods for calculating both liquid holdup and friction factor, and some chose to divide the flow conditions into patterns or regimes and develop separate correlations for each flow regime. The correlations are classified according to their complexity.[26] In Table 2, brief descriptions of all correlations considered for this model are presented. Also, we have taken into account the effect in the pressure drop of the fluid flow through chokes in the well surface.[27,28]

The deposition rate depends on the oil composition, fluid temperature, and external temperature around the pipe, flow conditions, pipe dimensions, and pressure. In our analysis of asphaltene deposition in the pipe, the region next to the wall, where the boundary layer flow, heat flux, and the radial component of the diffusion flux are related, is the key section of the model, where heat transfer with constant heat flux at the wall is considered at a given pressure drop. The radial temperature gradient induces a radial concentration gradient in the liquid phase, assuming that the phase diagram does not change with flow, which means that thermodynamic equilibrium is attained faster than any flow-related time scale. Of course, if the phase diagram can be modified by the flow, then a nonequilibrium thermodynamics model is necessary. Undoubtedly, such an approach is more appropriate, but for the multiphase-multicomponent modeling undertaken in this analysis, is the approach given in this work is a good first approximation. As the phase change (solids precipitation) occurs next to the wall, the liquid phase is depleted of dissolved solids in this layer, inducing a concentration gradient of dissolved solids directed toward the bulk fluid. Then the dissolved solids mass flux is induced toward the wall. The deposition of solids forms a solids deposit that can be subjected to removal by shear forces.

(26) Brill, J. P.; Beggs, H. D. *Two-Phase Flow in Pipes*, 6th ed.; University of Tulsa: Tulsa, OK, 1994.

(27) Omana, R. *SPE Prod. Eng.* Presented at the 44th Annual Fall Meeting, Denver, CO, September 1969; SPE No. 2682.

(28) Sachdeva, R.; Schmidt, Z.; Brill, J. P.; Blais, R. M. *SPE Prod. Eng.* Presented at the SPE Annual Technical Conference and Exhibition, New Orleans, LA, Oct 5−8, 1986; SPE No. 15657.

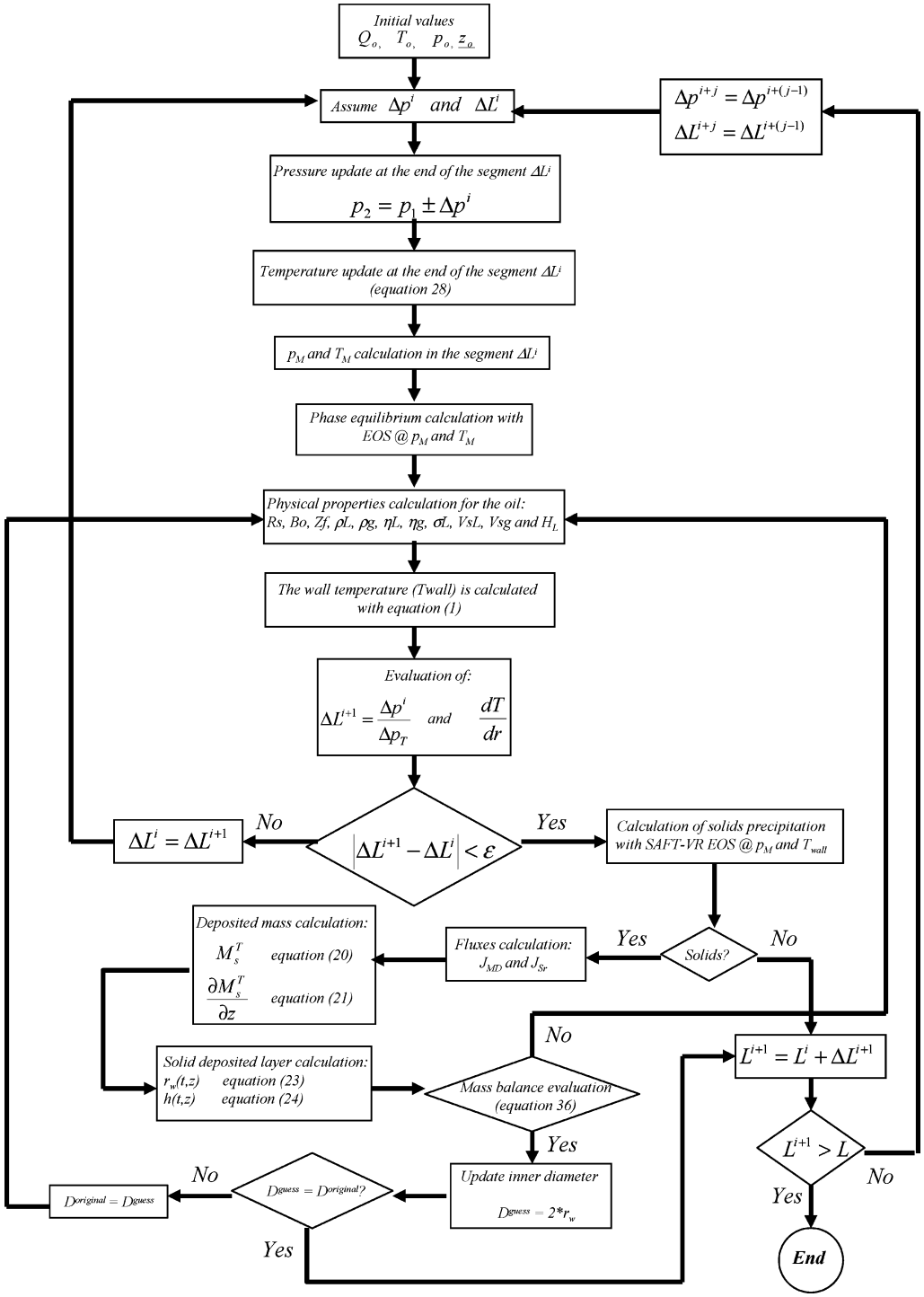

Figure 5. Computational procedure.

The molecular diffusion according to Fick's law is calculated for each mixture component, and the total mass flow is the sum of the component flows as:[29]

$$J_{\mathrm{MD}} = \sum_{i=1}^{n} {J_{\mathrm{MD}}}^{i} = -D\sum_{i=1}^{n}\frac{\partial \rho_{xi}}{\partial r} = -D\rho_{\mathrm{m}}\sum_{i=1}^{n}\left[-T\frac{\partial w_{\mathrm{s}i}}{\partial T} + (1 - w_{\mathrm{s}i})\frac{T}{\rho_{\mathrm{m}}}\frac{\partial \rho_{\mathrm{m}}}{\partial T}\right]\frac{1}{T}\frac{\partial T}{\partial r} \quad (10)$$

w_{si} is the solid fraction of the i component in the solid phase.

The removal of the deposition layer due to the shear forces acting on the wall surface ("shear-removal") is a function of the wall shear stress and the deposited mass. This mechanism, as suggested by Kern and Seaton,[30] can be expressed as follows:

$$J_{\mathrm{sr}} = A_1 \tau_{\mathrm{p}} {M_{\mathrm{S}}}^{\mathrm{T}}(t - \mathrm{d}t,z)\exp(-B_1/T) \quad (11)$$

Constants A_1 and B_1 depend on the oil composition, T is the average temperature in the interval, ${M_{\mathrm{S}}}^{\mathrm{T}}(t - \mathrm{d}t,z)$ is the deposited

(29) Svendsen, J. A. *AIChE J.* **1993**, *39*, 1377−1388.

(30) Kern, D. Q.; Seaton, R. E. *Brit. Chem. Eng.* **1959**, *4*, 258.

Table 3. Compositional Analysis for the Live Oil from the WA Well at 155 °C and 211.34 kg/cm²

component	molecular weight	global wt %	global mol %	mol %
CO2	44.010	0.49	1.20	1.20
H2S	34.080	0.04	0.12	0.12
N2	28.013	0.18	0.70	0.70
C1	16.043	5.01	34.05	34.05
C2	30.070	3.09	11.21	11.21
C3	44.097	2.87	7.10	7.10
i-C4	58.124	0.52	0.98	0.98
n-C4	58.124	1.69	3.17	3.17
i-C5	72.151	0.91	1.38	1.38
n-C5	72.151	1.41	2.13	2.13
C6	85.000	2.08	2.67	
methyl-cyclo-C5	84.160	0.42	0.54	
benzene	78.110	0.16	0.23	
cyclo-C6	82.150	0.28	0.38	3.81
C7	99.000	2.51	2.40	
methyl-cyclo-C6	98.190	0.60	0.66	
toluene	92.140	0.37	0.44	
C8	113.000	3.03	2.92	
ethyl-benzene	106.170	0.28	0.29	
M&P-xylen	106.170	0.22	0.23	
O-xylen	106.170	0.22	0.23	
C9	128.300	3.22	2.74	9.90
C10	134.000	3.74	3.04	
C11	147.000	3.25	2.41	
C12	161.000	2.72	1.84	
C13	175.000	2.56	1.59	
C14	190.000	2.32	1.33	10.22
C15+	206.000	2.17	1.15	
C16	222.000	1.83	0.90	
C17	237.000	1.67	0.77	
C18	251.000	1.53	0.66	
C19	263.000	1.48	0.61	4.09
C20	275.000	1.35	0.53	
C21	291.000	1.11	0.41	
C22	305.000	0.98	0.35	
C23	318.000	0.77	0.26	
C24	331.000	0.66	0.22	
C25	345.000	0.55	0.17	
C26	359.000	0.45	0.14	
C27	374.000	0.42	0.12	
C28	388.000	0.34	0.09	
C29	402.000	0.26	0.07	2.38
C30+	580.000	40.23	7.56	7.56
molecular weight =			108.96	
density =	0.6791		°API =	29.28

Table 4. Compositional Analysis for the Live Oil from the WB Well at 155 °C and 630.81 kg/cm²

component	molecular weight	global wt %	global mol %	mol %
CO2	44.010	0.42	1.05	1.05
H2S	34.080	0.01	0.02	0.02
N2	28.013	0.16	0.63	0.63
C1	16.043	5.10	35.37	35.37
C2	30.070	3.14	11.63	11.63
C3	44.097	3.13	7.89	7.89
i-C4	58.124	0.61	1.17	1.17
n-C4	58.124	2.06	3.94	3.94
i-C5	72.151	1.09	1.69	1.69
n-C5	72.151	1.65	2.54	2.54
C6	85.000	2.63	3.44	
methyl-cyclo-C5	84.160	0.43	0.57	
benzene	78.110	0.12	0.17	
cyclo-C6	82.150	0.31	0.42	4.60
C7	99.000	2.48	2.42	
methyl-cyclo-C6	98.190	0.58	0.66	
toluene	92.140	0.25	0.31	
C8	113.000	2.81	2.77	
ethyl-benzene	106.170	0.21	0.22	
M&P-xylene	106.170	0.26	0.28	
O-xylene	106.170	0.10	0.11	
C9	128.300	2.64	2.29	9.05
C10	134.000	2.88	2.39	
C11	147.000	2.38	1.80	
C12	161.000	1.89	1.31	
C13	175.000	1.68	1.07	
C14	190.000	1.39	0.81	7.39
C15+	206.000	1.27	0.69	
C16	222.000	1.03	0.52	
C17	237.000	0.75	0.35	
C18	251.000	0.62	0.27	
C19	263.000	0.55	0.23	2.06
C20	275.000	0.45	0.18	
C21	291.000	0.42	0.16	
C22	305.000	0.32	0.12	
C23	318.000	0.26	0.09	
C24	331.000	0.18	0.06	
C25	345.000	0.14	0.05	
C26	359.000	0.10	0.03	
C27	374.000	0.09	0.03	
C28	388.000	0.06	0.02	
C29	402.000	0.04	0.01	0.75
C30+	580.000	53.29	10.23	10.23
molecular weight =			111.29	
density =	0.7762		°API =	26.23

mass at a given time, and τ_P is the shear stress at the wall:

$$\tau_P = \frac{\Delta p}{L}\frac{r_w}{2} \tag{12}$$

r_w is the pipe effective radius, which includes the deposited solids width. Equation 11 stands for the shear removal mechanism, expressing that the mass flux from the deposit is a function of the deposited mass and wall shear stress, and the oil properties are taken into account through the two constants. This is a very general expression that has advantages, such as choosing the wall shear stress as the important variable. The wall shear stress is independent of the type of fluid since it was derived from linear momentum balance and is related to the flow strength.

The calculation of the width of the solid layer on the pipe walls involves the mass deposited at time t, $M_S^T(t,z)$, along the length of the pipe L from ($z = 0$ up to $z = L$):

$$M_S^T(t,z) = \sum_{i=1}^{n} M_S^i(t,z) = 2\pi\{\int_0^t\int_0^L [r_w(\sum_{i=1}^{n} J_{MD}^i|_{r=r_w} - J_{sr})]\, dz\, dt\} \tag{13}$$

Table 5. SARA Analysis for the Fluids of the WA and WB Wells

well	saturates (%)	aromatics (%)	resins (%)	asphaltenes (%)	insolubles in DCM (%)
WA	44.65	34.55	17.90	2.86	0.04
WB	46.48	34.34	17.74	1.43	0.01

where r_w is the effective pipe radius. The increase in deposited mass per unit length at time t is $\partial M_S^T/\partial z$:

$$\frac{\partial M_S^T}{\partial z} = \sum_{i=1}^{n}\frac{\partial M_S^i}{\partial z} = 2\pi\{\int_0^t [r_w(\sum_{i=1}^{n} J_{MD}^i|_{r=r_w} - J_{sr})]\, dt\} \tag{14}$$

The total deposited mass as a function of time is given by:

$$\frac{dM_S^T}{dt} = \sum_{i=1}^{n}\frac{dM_S^T}{dt} = 2\pi\{\int_0^L [r_w(\sum_{i=1}^{n} J_{MD}^i|_{r=r_w} - J_{sr})]\, dz\} \tag{15}$$

Finally, the inner effective pipe radius $r_w(t,z)$ and the width of the deposited layer $h(t,z)$ can be calculated using the previous equations.[10,29]

Calculation Procedure

The calculation procedure used to obtain the deposition of asphaltenes of a flowing multicomponent mixture involves the calculation of the pressure and temperature profiles in vertical, inclined, and horizontal tubes where multiphase correlations are used together with the corresponding phase diagram for asphaltenes (SAFT-VR equation of state). The corresponding iterative procedure for the whole calculation is depicted in Figure 5.

The calculation begins with the discretion of the pipe in a number of segments along the axial direction, and the determination of the temperature and pressure at the extreme of each segment. The model should satisfy primarily the heat balance together with the phase equilibrium relations, and thereafter, the model should predict a value of the pressure that must converge to the predetermined pressure value at each segment. The following steps complete the algorithm:

1. At a given pipe length where the pressure is known (p_1, L_1), a pressure drop is assumed for the next segment length (Δp^i and ΔL^i), in addition to the temperature of the reference segment (T_1), and the height of the controlled volume.

2. With these initial values of length and pressure, the pressure is updated at the end of the segment ($p_2 = p_1 \pm \Delta p^i$), where $\pm$ indicates the calculation direction.

3. With p_2, the PVT properties are determined to implement the Romero-Juarez correlation[31] for calculation of the fluid temperature (T_2), which is given by the equation:

$$T(z) = T_a + (T_1 - T_a)\exp(-Az) \tag{16}$$

where

$$A = \frac{\pi DU}{12\, W_f\, C_f} \tag{17}$$

In eqs 16 and 17, D is the pipe diameter, U is the global heat transfer coefficient, T_a is the surrounding temperature, z is the length, W_f is the mass flow rate, and C_f is the specific heat of the fluid. These equations are valid for horizontal or inclined wells. To calculate the temperature distributions in gas ducts, the temperature changes due to gas expansion as pressure decreases (Joule−Thompson effect) should be considered. In this case, eq 16 is substituted by the following expression:

$$T(z) = \left[T_1 - \left(T_a - \left(\frac{\vartheta}{A}\right)\frac{dp}{dz}\right)\right]\exp(Az) \tag{18}$$

where ϑ is the Joule−Thompson coefficient and dp/dz is the pressure gradient. In vertical pipes, according to the Romero-Juarez procedure,[31] the axial temperature profile can be determined using the Ramey equation:[32]

$$T(z) = T_{wf} - Ge\{A[1 - \exp(-z/A)] - z\} \tag{19}$$

where

$$A = \frac{86\,400 W_f C_f (K_e + DF_T)}{2\pi DK_e U} \tag{20}$$

F_T is a time-dependent function valid for times less than 400 days:

$$\log F(t) = 0.31333 \log Y - 0.06(\log Y)^2 + 0.006666(\log Y)^3 \tag{21}$$

$$Y = \frac{552t}{D^2}$$

and hence:

$$F_T = 10^{\log f(t)} \tag{22}$$

Otherwise, if $t \geq 400$ days, then $F_T = 1$.

In eqs 19 and 20, K_e and Ge are the geothermal conductivity and gradient of the fluid, T_{wf} is the bottom temperature, and t is the current time.

4. Once the pressure and temperature at the extremes are known, the pressure, temperature, and mean length of the segment are determined (p_M, T_M, and L_M).

5. According to these mean values, the PVT properties of the mixture are determined (Rs, Bo, Z_f, ρ_L, ρ_g, η_L, η_g, σ_L, V_{sL}, and V_{sg}). Thereafter, the total pressure drop (Δp_T) in the segment is calculated according to eq 9; the liquid holdup (H_L), the mixture density, and the flow patterns are estimated; and the Reynolds number (Re) of the fluid is estimated.

6. The wall temperature (T_{wall}) is calculated with eq 1.

7. The length increase is evaluated according to $\Delta L^{i+1} = \Delta p^i / \Delta P_T$ for the segment considered. If ΔL^i and ΔL^{i+1} are equal, the procedure continues to step 8, otherwise step 2 is followed.

8. The radial temperature gradient (dT/dr) is calculated using the approximation $dT/dr \approx \Delta T/\Delta r$, where $\Delta T = T_{wall} - T_{fluid}$ and Δr is the width of the boundary layer.

9. The wall temperature and mean segment pressure T_{wall} and p_M are used to calculate the phase equilibrium, which renders the properties and amounts of the fluid phases (liquid and gas) and solid phase (asphaltenes). In the case of the appearance of solid fractions, the procedure continues to step 10, otherwise it continues to step 19.

10. The mass flux of the solid-phase components (eq 10) and the solids amount removed by the shear stress (eq 11) are calculated.

11. The total mass deposited on the pipe inner wall for a given time at a distance z from the entrance section (eq 14) is calculated for each component in the solid phase, according to:

$$\frac{\partial M_S{}^i(t+\Delta t,z)}{\partial z} = \frac{\partial M_S{}^i(t,z)}{\partial z} + 2\pi \int_t^{t+\Delta t} r_w(t,z)(J_{MD}{}^i - J_{SR})\, dt \tag{23}$$

12. The effective pipe radius $r_w(t,z)$ and the width of the deposited layer $h(t,z)$ are updated.

13. The deposited solid mass for each component along the length of the pipe at time $t + \Delta t$ is calculated according to:

$$M_S{}^i(t+\Delta t) = M_S{}^i(t) + \int_0^L \frac{\partial M_S{}^i(t+\Delta t,z)}{\partial z}\, dz \tag{24}$$

14. The total amount of solids deposited at time $t + \Delta t$ is also calculated:

$$M_S{}^T(t+\Delta t) = \sum_{i=1}^{n} M_S{}^i(t+\Delta t) \tag{25}$$

15. The amount of deposited solids per unit area of the pipe clean inner wall is given according to:

(31) Romero-Juarez, A. *JPT* **1979**, 763−768.
(32) Ramey, H. J. *Trans. AIME* **1962**, 225.

$$m_S(t + \Delta t) = \frac{M_S^T(t + \Delta t)}{2\pi r_o L} \quad (26)$$

16. The mass balance for the reference segment is carried out:

$$(\rho_m Q)_{i+1} = (\rho_m Q)_i - \frac{dM_S^T}{dt} \quad (27)$$

The first term of eq 27 is the fluid mass entering the segment with position $i + 1$ from position i. On the right-hand side, the first term stands for the fluid mass exiting position i and the second term is given by eq 15, depending on the particular case considered. If eq 27 holds, then the procedure continues to step 19, otherwise $p_M^* = p_M \pm \delta$, and it continues to step 9.

18. The new pipe diameter, which considers the deposited layer, is updated ($D = 2r_w$).

19. The upper extremes of the intervals $p_2 = p_1 + \Delta L^{i+1}$ and $L_2 = L_1 + \Delta L^{i+1}$ are calculated. If the total length of the pipe is reached, the calculation procedure is concluded, otherwise, we set $p_1 = p_2$ and $L_1 = L_2$ and follow step 2.

Results and Discussion

A working example considers the analysis of the deposition problem in two oil wells from a productive oil field of PEMEX[12] in Southeast Mexico, where measured $P-T$ profiles versus depth of these (plugged) wells are available. This is a naturally fractured reservoir, with a static reservoir pressure (*Pws*) and temperature of 920 kg/cm^2 and 155 °C, respectively. This reservoir produces a light (32 °API) oil with an average bubble point pressure of 132 kg/cm^2 and the average *GOR* of 100 m^3/m^3.[33] Experimental data on the phase behavior of asphaltene precipitation for the reservoir fluids are available, which include the asphaltene phase boundaries (i.e., asphaltene precipitation envelope), the extended compositional characterization of each (live) oil, and the SARA analysis (i.e., weight fractions of the saturated hydrocarbons, aromatics, resins, and asphaltenes), together with a full set of PVT analyses for each fluid.[34] The wells studied will henceforth be called wells WA and WB. In Tables 3 and 4, the extended compositional analyses for the oil of each well are presented, respectively. Table 5 presents the corresponding SARA analyses. As observed, the produced oil in well WA contains larger amounts of asphaltenes and resins than the oil in WB.

Figure 6a,c shows the measured phase boundaries (upper, lower, and saturation pressure curve) for the live oils in the two wells, respectively. There are two sets of initial data to input to the model: the first one contains the thermodynamic information to characterize the oil. The second one contains the information regarding the well geometry and current operation conditions. Thermodynamic properties include the components' critical properties (pressure, temperature, volume, and acentric factor), temperature and heat of fusion, molecular weight, relative density of each component, and the recorded temperature. Finally, the global composition of the mixture (obtained directly from the chromatographic data) is required. Tables 6 and 7 show the corresponding values of the study cases (WA and WB, respectively). Finally, to complete the fluid characterization, the molecular weight and the relative density of the C_{7+} fraction are needed to define a determined number of pseudo components. The values used for these oils include a molecular weight of 284.36 g/gmol with relative density of 0.805 g/cm^3.

Once the composition and critical properties of the mixture are defined, the next step is to fit the SAFT-VR equation of state to the phase behavior data (asphaltene precipitation envelope, APE) determined experimentally (Figure 6a,c). This requires as an input the phase boundary and the compositional characterization of the oils (Tables 3 and 4 and the SARA analysis, Table 5). To obtain the calculated onset and saturation pressures with the SAFT-VR EOS, the two-stage calculation method described by Buenrostro-Gonzalez et al.[21] is performed. Results of this fit are shown in Figure 6b,d for each well, respectively (ESDA stands for the upper phase boundary of asphaltene deposition, ESIA stands for the lower phase boundary, and p_b is the saturation pressure curve). The continuum line represents the better fit to the upper boundary data, while the blue curve represents the best fit obtained to the saturation pressure data. Table 8 presents the values of the fitting parameters of the SAFT-VR EOS.

Oil wells WA and WB are two out of three wells selected by PEMEX from an oil sampling operation carried out in the field for this study (each well has a different physical location in the reservoir). As shown in Tables 3−5, the produced fluids from these wells have significant differences in composition and asphaltene/resin content. Despite this "multisample" situation in the reservoir, it is particularly rewarding to see from Figure 6b,d that the SAFT-VR EOS used in this work was able to give a reasonable match of both bubble point and upper onset pressures of the *two* reservoir fluids, using the *same* set of EOS parameters (similar results for the third oil well—not shown here—were obtained). Certainly, a much better description to the experimental data of Figure 6 would have been obtained if individual EOS matches to each APE data set of Figure 6 would have been performed. Such an approach was not follow here. Instead, a single EOS representation for the entire reservoir was therefore perferred in this work.

Regarding the well geometry, the input information required is the well trajectory as a function of depth to calculate its length and the angle departures from the vertical. The production well is divided into a number of segments, assigning the mean angle for each segment from the gyroscopic record. Tables 9 and 10 contain the analysis results for each study case. In addition, the production information for each well is disclosed in Table 11. This includes the pressure and temperature at the bottom and top sections, flow rate, *GOR*, contraction diameter, water production, and pressure and temperature at standard conditions.

The process was simulated considering an elapsed time of 500 days for asphaltene deposition in multiphase flow. To ensure reliable predictions at conditions different from the current production conditions from the model, we first match the measured $P-T$ profiles of the flowing wells by varying slightly the values of the roughness coefficient and the global heat transfer coefficient. The initial value for roughness is 0.001 (clean pipe), which was subsequently changed. The final value for the roughness is shown in Tables 9 and 10. The results of the fit are shown in Figure 7a,b. The maximum error of the fit is less than 2% in pressure. The next step includes the calculation of asphaltene adhesion and plugging in the production well at both the current production conditions and at a set of variations to them (sensibility analysis). Results are presented in Figure 8a,c for each well, considering

(33) Salazar, B. M.; Tejeda, F. P.; Lozada, M. A. *Revista AIPM Comalcalco*; Reporte Interno; PEMEX: Tabasco, México, 2000.

(34) Lira-Galeana, C.; Ramírez-Jaramillo, E.; Buenrostro-González, E.; Ortega-Rodríguez, A. Internal Report; F. 53991; Instituto Mexicano del Petróleo: Mexico, 2004.

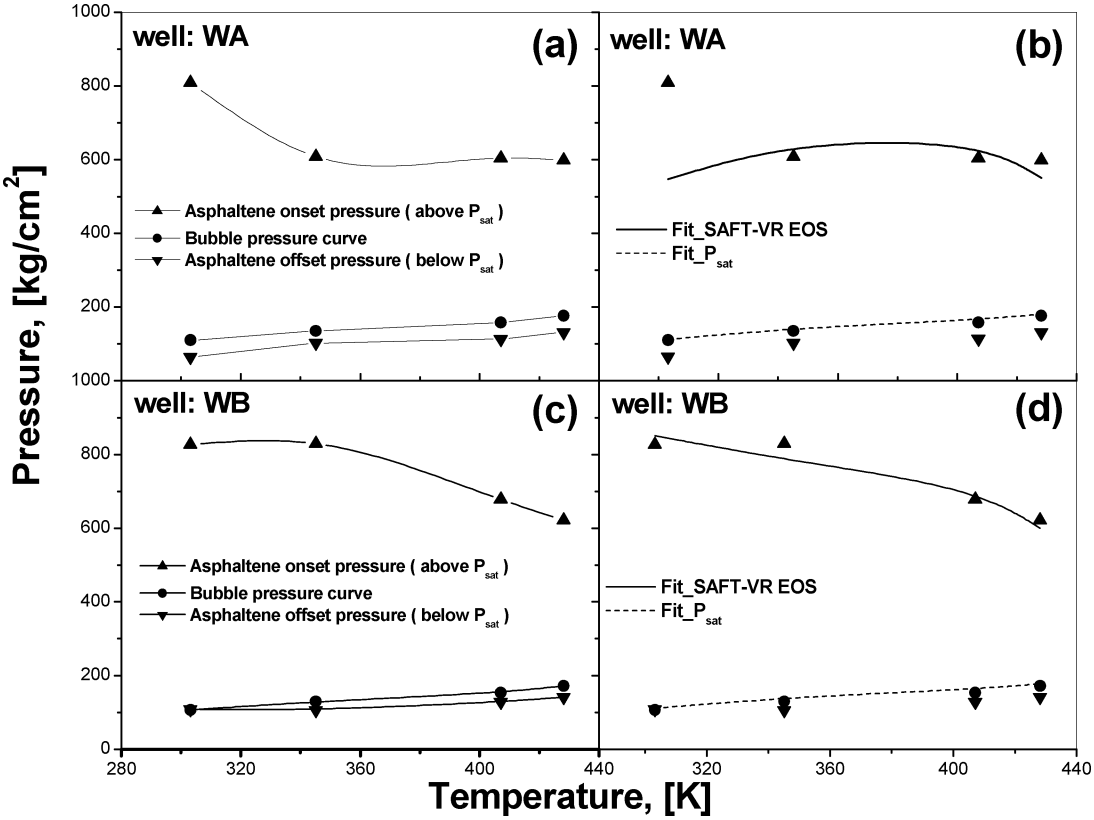

Figure 6. (a) Asphaltene precipitation envelope (APE) for the WA well. (b) SAFT-VR EOS representation of the experimental APE of the WA oil fluid. (c) APE for the WB well. (d) SAFT-VR EOS representation of the experimental APE of the WB oil fluid.

Table 6. Compositional Characterizations for the Oil from the WA Well

component	WM	T_c (K)	P_c (kg/cm^2)	V_c (kg/kg mol)	ω_i	T_f (K)	Δh (kJ/kmol)	ρ_i (kg/m^3)	T_ρ (K)	TB (K)	z_i
N_2	28.01	126.2	2.383	89.90	0.039	90.70	941.4	804	78.0	77.40	0.0069
CO_2	44.01	304.2	5.185	93.90	0.225	90.70	941.4	0.0	0.0	265.1	0.0119
H_2S	34.08	373.2	6.285	98.60	0.284	90.70	941.4	993	214.0	213.5	0.0011
C_1	16.04	190.6	3.234	99.20	0.008	90.70	941.4	425	112.0	111.6	0.3369
C_2H_6	30.07	305.4	3.430	148.3	0.099	90.00	2923	548	183.0	184.6	0.1109
C_3H_8	44.09	369.8	2.988	203.0	0.153	86.00	3604	582	231.0	231.1	0.0705
i-C_4H_{10}	58.12	408.2	2.566	263.0	0.183	138.0	3786	802	293.0	261.4	0.0097
C_4H_{10}	58.12	425.2	2.636	255.0	0.193	138.0	3786	579	293.0	272.7	0.0317
i-C_5H_{12}	72.15	460.4	2.383	306.0	0.227	97.00	4167	620	293.0	301.0	0.0139
C_5H_{12}	72.15	469.7	2.369	304.0	0.251	97.00	4167	626	293.0	309.2	0.0216

Table 7. Compositional Characterizations for the Oil from the WB Well

component	WM	T_c (K)	P_c (kg/cm^2)	V_c (kg/kg mol)	ω_i	T_f (K)	Δh (kJ/kmol)	ρ_i (kg/m^3)	T_ρ (K)	TB (K)	z_i
N_2	28.01	126.2	2.383	89.90	0.039	90.70	941.4	804	78.0	77.40	0.014
CO_2	44.01	304.2	5.185	93.90	0.225	90.70	941.4	0.0	0.0	265.1	0.0097
H_2S	34.08	373.2	6.285	98.60	0.284	90.70	941.4	993	214.0	213.5	0.0005
C_1	16.04	190.6	3.234	99.20	0.008	90.70	941.4	425	112.0	111.6	0.3349
C_2H_6	30.07	305.4	3.430	148.3	0.099	90.00	2923	548	183.0	184.6	0.0981
C_3H_8	44.09	369.8	2.988	203.0	0.153	86.00	3604	582	231.0	231.1	0.068
i-C_4H_{10}	58.12	408.2	2.566	263.0	0.183	138.0	3786	802	293.0	261.4	0.0106
C_4H_{10}	58.12	425.2	2.636	255.0	0.193	138.0	3786	579	293.0	272.7	0.0368
i-C_5H_{12}	72.15	460.4	2.383	306.0	0.227	97.00	4167	620	293.0	301.0	0.0165
C_5H_{12}	72.15	469.7	2.369	304.0	0.251	97.00	4167	626	293.0	309.2	0.0254
C_6H_{12}	86.18	507.5	2.116	370.0	0.299	97.00	4167	659	293.0	341.9	0.0714

that the reported values are average values of the deposit highest width, to smooth the high dispersion of resulting magnitudes. This criterion is used subsequently in the following discussion.

The wells are of the so-called directional type,[35] ones of medium and large length (1000 and 2500 m) producing at 3996 m (WA) and 4035 m (WB), with diameter reduction due to TR of 0.178 m (7 in.) and of 0.244 m ($9^{5/8}$ in.), respectively.

As observed in the previous figures, asphaltene deposition is apparent at different depths of the production well. For well WA, the deposit layer initiates at a depth of 2488 m and ends at 3720 m at the current production conditions (7712 BDP or 0.0142 m^3/s). The deposit width is 0.007 m (0.27 in.), 10% of

(35) Bourgoyne, A. T.; Milheim, K. K.; Chenevert, M. E.; Young, F. S. *Applied Drilling Engineering*; SPE Textbook Series; Society of Petroleum Engineers: Houston, TX, 1991; pp 351−453.
(36) Zapata-González, C.; Lira-Galeana, C.; Firó-Reyes, J.; Lucero-Aranda, F.; García-Hernández, F. *Ingeniería Petrolera* **1999**, *38*, 58.
(37) Poettmann, F. H.; Carpenter, P. G. *Drilling and Production Practices API* **1952**, 257−317.
(38) Baxendell, P. B.; Thomas, R. *JPT* **1961**, 1023−1028.
(39) Fancher, G. H.; Brown, K. F. *SPE Prod. Eng.* **1963**, 59−69.
(40) Hagedorn, A. R.; Brown, K. E. *JPT* **1965**, 475−484.

Table 8. Values for the SAFT-VR Equation of State Parameters for the Oils Fluids of the WA and WB Wells

	well	
parameter	WA	WB
HA	11270	11270
HR	1891	1891
EA AA	1523.67	1481
EA RR	2406.97	2486.54
Lamda AA	4.28	4.07
Lamda AR	4.166	4.166
Lamda RR	6.3	6.36
Kappa AA	0.05	0.05
Kappa AR	0.05	0.05
LR	10	10
diamR	5	5
diamA	17	17
pmA	3129	3129
densA	1120	1120
pmR	571	571
densR	900	900
%wA	2.9	1.43
%wR	17.9	17.74
Nsites A	2	2
Nsites R	1	1
Etapure A	0.5545	0.5545
Etapure R	0.6213	0.6213

Table 9. Production Tubing (*PT*) Configuration for the WA Well

inside diameter (m)	external diameter (m)	length *PT* (m)	roughness	inclination angle (deg)
0.143*	0.143	414.9	0.009	1.1
0.153	0.178	407.8	0.009	2.8
0.153	0.178	615.6	0.009	22.5
0.076	0.089	470.1	0.005	25.2
0.076	0.089	3502.9	0.006	0.4

Table 10. Production Tubing (*PT*) Configuration for the WB Well

inside diameter (m)	external diameter (m)	length *PT* (m)	roughness	inclination angle (deg)
0.178[a]	0.159	1465.4	0.0099	28.0
0.100	0.114	711.1	0.0011	22.3
0.100	0.114	256.0	0.0014	23.4
0.100	0.114	624.1	0.0022	20.9
0.100	0.114	706.7	0.006	8.2
0.100	0.114	1743.0	0.0052	0.201

[a] Open hole.

the effective inner diameter. With an increase in flow rate to 5000 BPD (0.0092 m^3/s), the width increases to 0.028 m (1.09 in.), 40% of the effective inner pipe diameter. However, the location of the deposit shifts to larger depths (5381 to 3724 m, 1657 m length) reaching the *CT* (coiled tubing), where the maximum width is observed. With further reduction in the flow rate (3000 BDP or 0.0055 m^3/s), the deposit shows up at a depth of 5500 m up to 4732 m, with a length of 769 m. For decreasing flow rates, the location of the deposit tends to shift to larger depths, near the *CT* section, and the deposit width reaches 0.0127 m (0.5 in.), representing 7% of the *CT* diameter. On the other hand, if the flow rate is increased, the location of the deposit shifts to the surface section of the well, initiating at 3115 m (9000 BPD or 0.0165 m^3/s) and 2012 m (12 000 BPD or 0.022 m^3/s). The deposit length in both cases is approximately 1400 m.

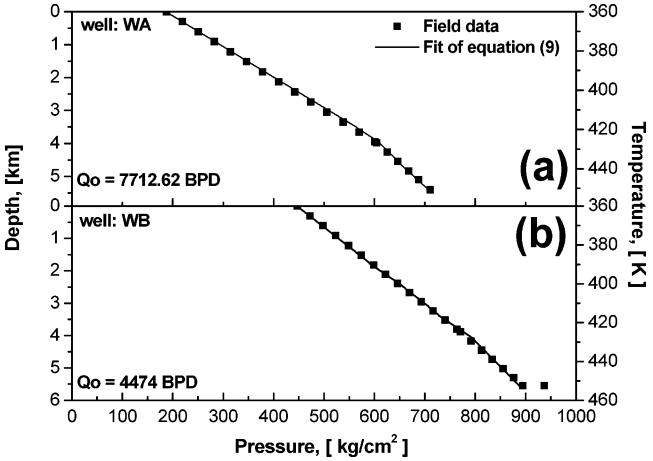

Figure 7. (a) Axial pressure profile calculated for the WA well. (b) Axial pressure profile calculated for the WB well.

As per well WB, the asphaltene deposit initiates at a depth of 1640 m and ends at 2810 m. The layer width is 0.0124 m (0.49 in.), about 18% of the effective inner diameter. Under any flow rate condition, a shift in the deposit layer is predicted, but the predictions further indicate a constant value of the deposit width. It is important to note that, according to model predictions, for a flow rate of 6500 BDP (0.012 m^3/s), the solid deposit reaches the well exit.

Another observation is that in most cases the width profile presents a highly diffusive structure, resulting from a fine discretion (every 8 m) of the production well, generating a wealth of data.

Further sensitivity calculations were made including changing the diameter and maintaining the flow rate constant. The deposition profile along the well is presented in Figure 8b,d. The asphaltene deposit shifts with changes in diameter. The behavior of well WB, the diameter change from 0.0889 m ($3^{1/2}$ in.) to 0.073 m ($2^{7/8}$ in.) induces a shift in the deposit layer toward the well surface (from 3720 to 2480 m) with slowly decreasing width (0.004318 m mean value, or 6% of the effective pipe inner diameter). When the diameter increases from 0.0889 m ($3^{1/2}$ in.) to 0.1143 m ($4^{1/2}$ in.), the deposit layer tends to move to larger depths (from 3720 to 5013 m) with increasing width (mean value of 0.0312 m, 18% of the effective inner pipe diameter, to a mean value of 0.0112 m, 15% of the effective inner pipe diameter).

The behavior of the WB well (Figure 8d) is similar, although the length shift is smaller than in the previous cases. The width of the deposit layer increases to 0.0173 m (0.68 in.), a 25% of the effective inner pipe diameter.

Since these calculations on real production wells are novel, it is difficult to compare these predictions with standard profiles obtained by other methods elsewhere. However, it is possible to determine the solid onset pressure if we couple the solid precipitation envelope with the pressure−temperature−depth production profile in the same diagram. The intersection point is associated with the solid onset pressure.[36] This (approximate) procedure represents an alternative way of estimating the well depth at which potential solid deposits would begin. The results obtained in this work compares satisfactorily with this methodology, as shown in following figures.

(41) Duns, H.; Ros, N. C. J. *Proceedings of the Sixth World Petroleum Congress*, Frankfurt, June 19−26, 1963; Section II, paper 22-PD6.
(42) Orkiszewski, J. *JPT* **1966**, *19*, 829−838.
(43) Beggs, H. D.; Brill, J. P. *JPT Trans.* **1973**, *255*, 607.
(44) Dukler, A. E.; Baker, O.; Cleveland, R. L.; Hubbard, M. G.; Wicks, M. *Research Results, Monograph NX-28*; University of Houston: Houston, TX, 1969.
(45) Mukherjee, H.; Brill, J. P. *J. Energy Resour. Technol.* **1985**.
(46) Aziz, K.; Govier, G. W.; Fogarasi, M. *J. Can Pet. Technol.* **1972**, 38−48.
(47) Cullender, M. H.; Smith, R. V. *Trans. AIME* **1956**, 207.

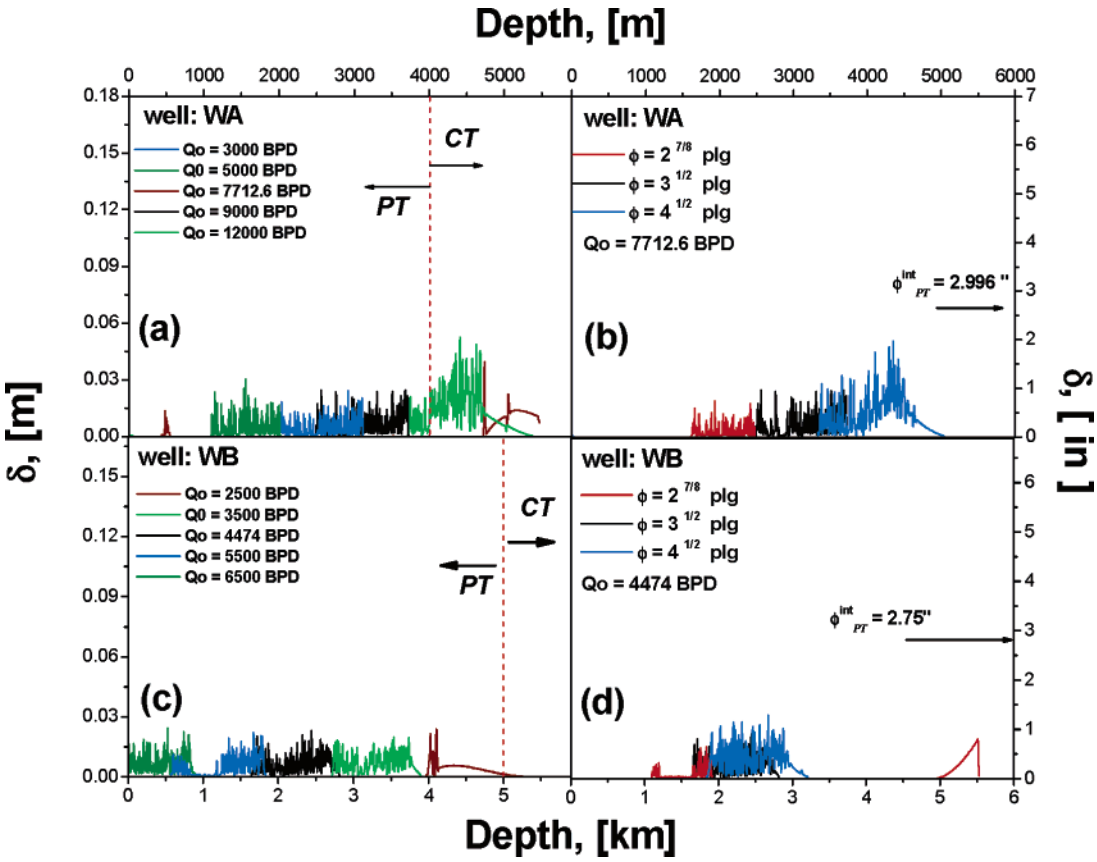

Figure 8. (a) Deposited asphaltene layer thickness as a function of the axial coordinate for different oil flow rate for the WA well. (b) Deposited asphaltene layer thickness as a function of the axial coordinate for different inner diameter tubing for the WA well. (c) Deposited asphaltene layer thickness as a function of the axial coordinate for different oil flow rate for the WB well. (d) Deposited asphaltene layer thickness as a function of axial coordinate for different inner diameters tubing for the WB well.

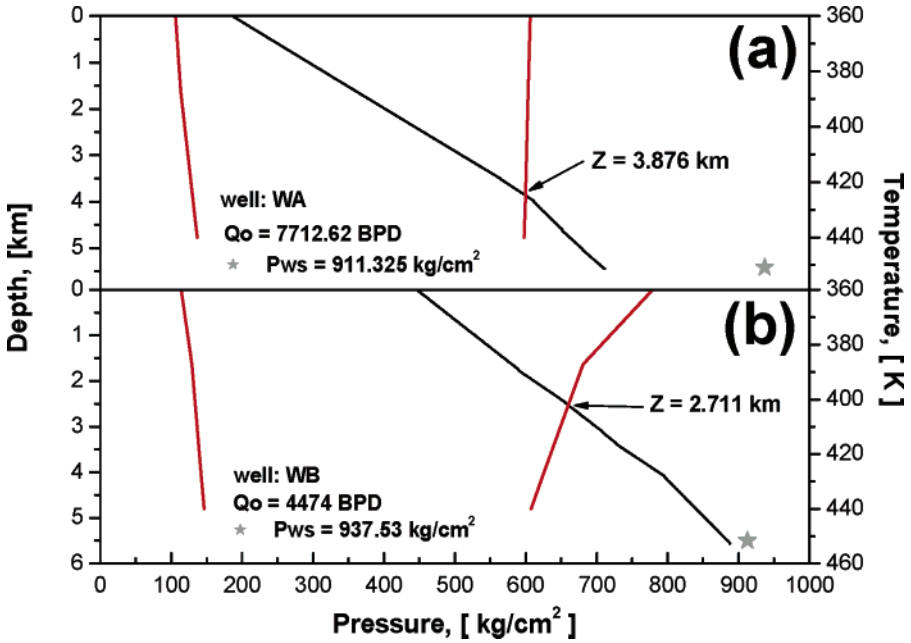

Figure 9. (a) Zapata-González et al.[36] method applied to the WA oil well. (b) Zapata-González et al.[36] method applied to the WB oil well.

Table 11. Production Parameters for the WA and WB Wells

	production parameters							
	U (kJ/h•m²•K)			*Tsc*	*Psc*	Q_o	GOR	choke
well	bottom	surface	%H_2O	(K)	(kg/cm²)	(m^3/s)	(m^3/m^3)	(m)
WA	51.1	29.6	0	301.2	14.7	0.01419	110	0.0159
WB	51.1	29.6	0	301.2	14.7	0.00823	110	0.0095

In Figure 8a, the deposit layer for the WA well calculated using this model initiates at a depth of 3720 m; while using the methodology (Figure 9a) a depth of 3876 m is predicted. The total length of the well is 4000 m, and thus the difference in the two predicted values is approximately 4%.

In Figure 8c, the deposit layer for the WB well initiates at a depth of 2810 m; while using the methodology (Figure 9b) a depth of 2711 m is predicted. The length of the pipe in this case is 4047 m, a 2.4% difference. In both wells, the bubble-point-pressure depth correlated well with deposit location, as expected.

In summary, results indicate that the two wells present deposit formations of asphaltenes located at various depths. As the static bottom pressure diminishes, the deposit shifts to larger depths, at the *CT* level, reaching depths near the bottom.

Conclusions

A flow model that couples transport phenomena, multiphase flow, and phase equilibria of hydrocarbon mixtures has been developed and tested.

Representative wells from an oil field with proven deposition problems were analyzed with this model. According to deposition data in these wells, the width of the deposition layer is not larger than 15% of the effective inner pipe diameter of the production well, indicating that the problem of solids deposition is bound to the initial stage of development.

A sensitivity analysis made on the operation variables indicates that for variable flow rate and fixed diameter, when the flow rate is decreased, the deposition layer shifts to larger depths, and vice versa. The mean width of the deposit increases slowly as the flow rate is varied, indicating that the growth rate of the deposit will remain constant independent of the flow rate. When the diameter is varied, a behavior similar to that when the flow rate is varied is predicted.

Predictions of the model were compared to those of other (approximate) methodologies. Agreement with those by Zapata-González et al.[36] is apparent at the level of the $P-T$ profiles available from field measurements.

Strategies should develop for the prevention and remedies of solids deposition. Specific techniques are used for the deposition control at the $P-T$ level, such as magnetic tools, chemicals injection, electrocentrifuged pumping, microorganisms, and the control of production variables.

The flow simulator developed here allows the calculation of the deposition profiles of asphaltenes, according to temperature and pressure profiles of a multiphase flow of liquid, gas, and asphaltene aggregates. The profiles are predicted as a function of time and give the location of the deposit. The knowledge of the dynamics of growth of the solids deposit is an important aspect to assess in well productivity.

Acknowledgment. This work was supported by the Mexican Institute of Petroleum's projects F.53910, F.53909 and F.53991. PEMEX E&P is thanked for providing oilfield data and fruitful discussion throughout this work.

Nomenclature

A = Inner surface (m^2)
A_H = Helmholtz free energy (J)
A_1, B_1 = Constants (dependent on the oil composition)
Bo = Oil formation volume factor at bubble point (res m^3/std m^3)
C_f = Specific heat of the fluid (J/kg·K)
C_p = Specific heat capacity of the mixture (J/kg·K)
C_1 = Constant characteristic of the oil (N)
CT = Coiled tubing
D = Pipe diameter and length (m)
D = Rate deformation tensors
$densA$ = Molecular number density of asphaltene ($1/m^3$)
$densR$ = Molecular number density of resins ($1/m^3$)
$diamA$ = Hard sphere diameter for the aspahaltene molecule (nm)
$diamR$ = Hard sphere diameter for the resin molecule (nm)
D_m = Average diffusion coefficient (m^2/s)
$EA\ AA$ = Association energy for the asphaltene molecule (J)
$EA\ RR$ = Association energy for the resin molecule (J)
$Etapure\ A$ = Packing fraction for the asphaltene molecule
$Etapure\ R$ = Packing fraction for the resin molecule
F_T = Time-dependent function in eq 31
F_w = Solids weight fraction
Ge = Geothermal gradient of the fluid (K/m)
GOR = Gas/oil ratio (m^3/m^3)
$h(t,z)$ = Width of the deposited layer (m)
HA = Hamaker constant for asphaltene (J/m^6)
h_{in} = Heat transfer coefficient (W/m^2·K)
H_L = Liquid holdup
HR = Hamaker constant for resins (J/m^6)
J_{MD} = Mass flux ($kg/s·m^2$)
J_{sr} = Removal rate ($kg/s·m^2$)
k = Boltzmann's constant (J/K)
k_{an} = Thermal conductivity of the annulus (W/m·k)
$Kappa\ AA$ = Shape of the attractive potential between asphaltene−asphaltene
$Kappa\ AR$ = Shape of the attractive potential between asphaltene−resin
k_b = Thermal conductivity of the mixture (W/m·k)
k_{ca} = Thermal conductivity of the casing (W/m·k)
k_{cem} = Thermal conductivity of the cement (W/m·k)
K_e = Geothermal conductivity ($kg·m/s^3$·K)
k_{oil} = Thermal conductivity of the oil (W/m·k)
k_p = Thermal conductivity of the pipe (W/m·k)
k_{res} = Thermal conductivity of the reservoir (W/m·k)
k_s = Thermal conductivity of the solids deposited (W/m·k)
L = Pipe length (m)
$Lamda\ AA$ = Range of the attractive potential between asphaltene−asphaltene
$Lamda\ AR$ = Range of the attractive potential between asphaltene−resin
$Lamda\ RR$ = Range of the attractive potential between resin−resin
LR = Segment number in the resin molecule
MW = Molecular weight (kg/kmol)
$M_S^T(t,z)$ = Total mass deposited (kg)
$m_S(t)$ = Deposited solid per unit area (kg/m^2)
n = Total number of components in the mixture
N_m = Number of molecules
$Nsites\ A$ = Number of association sites for the asphaltene molecule
$Nsites\ R$ = Number of association sites for the resin molecule
P_b = Saturation pressure (kg/cm^2)
P_c = Critical pressure (kg/cm^2)
P_M = Average pressure in the segment (kg/cm^2)
pmA =Asphaltene molecular weight (g/mol)
pmR = Resin molecular weight (g/mol)
P_o = Pressure (kg/cm^2)
Pr = Prandtl number
PT = Production tubing
Pws = Static bottom well pressure (kg/cm^2)
Q = Heat flux ($J/s·m^2$)
Q_o = Flow rate (BPD)
r = Radial distance (m)
Re = Reynolds numbers
R_o = Inner radius of clean tube (m)
R_s = Solution gas-oil ratio (scf/STB)
$r_w(t,z)$ = Effective pipe radius (includes deposited solids layer) (m)
t = Time (day)
T = Temperature (K)
T_a = Surrounding temperature (K)
T_B = Normal boiling temperature (K)

T_o = Inlet temperature (K)
T_c = Critical temperature (K)
T_f = Melting point temperature of component i (K)
T_{fluid} = Mean temperature in the core (K)
T_M = Average temperature in the segment (K)
T_{wall} = Wall temperature of the pipe (K)
T_{wf} = Bottom temperature (K)
T_ρ = Temperature at which density was measured (K)
T_1 = Reference temperature (K)
U = Global heat transfer coefficient (kg/s^3·K)
V = Molar volume (m^3)
V_c = Critical volume (m^3)
V_{sg} = Superficial velocity of the gas phase (m/s)
V_{sL} = Superficial velocity of the liquid phase (m/s)
W_f = Mass flow rate (kg/s)
w_{si} = Solid fraction of the i component in the solid phase
z = Axial distances (m)
z_i = Mole fraction of component i in the mixture
Z_f = Compressibility factor at critical point
z_o = Feed composition

Greek Letters

β = Caloric resistance of asphaltene
Φ_{solid} = Solid fraction
$\dot{\gamma}$ = Shear rate (s^{-1})
$\lambda_1, \lambda_2, \lambda_3$ = Parameter constants
Δh = Heat of fusion (kJ/mol)
δ = Deposited solid layer thickness (m)
ϵ = Tolerance value
η_b = Viscosity (kg/m·s)
η_{liq} = Suspension viscosity (kg/m·s)
η_L = Viscosity of the liquid phase (kg/m·s)
η_g = Viscosity of the gas phase (kg/m·s)
ρ_i = Density of the component i (kg/m^3)
ρ_m = Density of the mixture (kg/m^3)
ρ_s = Density of the solid phase (kg/m^3)
ρ_L = Density of the liquid phase (kg/m^3)
ρ_g = Density of the gas phase (kg/m^3)
ψ = Association parameter
ϑ = Joule−Thompson coefficient
σ_L = Interface tension
τ = Stress deformation tensors (kg/m^2)
τ_P = Shear stress at the wall (kg/m^2)
$(\Delta P/\Delta L)$ = Pressure drop (kg/cm^2/m)
ω_i = Acentric factor
$\%wA$ = Weight fraction of asphaltene in the mixture
$\%wR$ = Weight fraction of resin in the mixture

EF050262S